ACS APPLIED MATERIALS & INTERFACES

Research Article

www.acsami.org

Electrospun Ni-Added SnO_2–Carbon Nanofiber Composite Anode for High-Performance Lithium-Ion Batteries

Dongha Kim,[†] Daehee Lee,[†] Joosun Kim,*[,‡] and Jooho Moon*[,†]

[†]Department of Materials Science and Engineering, Yonsei University, 50 Yonsei-ro Seodaemun-gu, Seoul 120-749, Republic of Korea

[‡]Center for Energy Materials Research, Korea Institute of Science and Technology, Seoul 136-791, Republic of Korea

Supporting Information

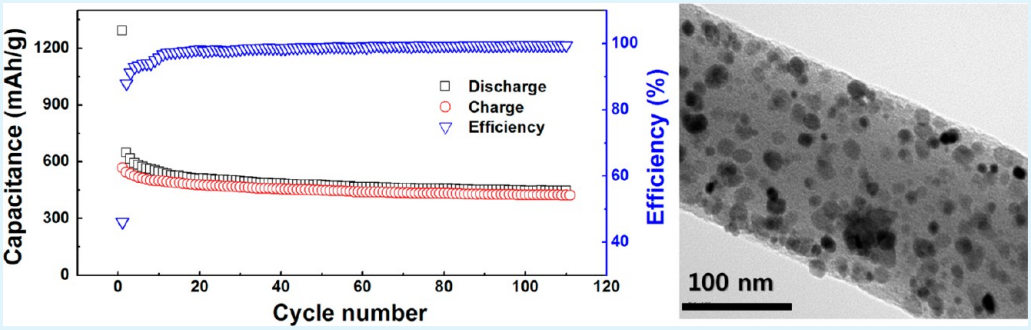

ABSTRACT: The SnO_2 anode is a promising anode for next-generation Li ion batteries because of its high theoretical capacity. However, it exhibits inherent capacity fading because of the large volume change and pulverization that occur during the charge/discharge cycles. The buffer matrix, such as electrospun carbon nanofibers (CNFs), can alleviate this problem to some extent, but SnO_2 particles are thermodynamically incompatible with the carbon matrix such that large Sn agglomerates form after carbonization upon melting of the Sn. Herein, we introduce well-dispersed nanosized SnO_2 attached to CNFs for high-performance anodes developed by Ni presence. The addition of Ni increases the stability of the SnO_2 such that the morphologies of the dispersed SnO_2 phase are modified as a function of the Ni composition. The optimal adding composition is determined to be Ni:Sn = 10:90 wt % in terms of the crystallite size and the distribution uniformity. A high capacity retention of 447.6 mA h g^{-1} after 100 cycles can be obtained for 10 wt % Ni-added SnO_2–CNFs, whereas Ni-free Sn/SnO_2–CNFs have a capacity retention of 304.6 mA h g^{-1}.

KEYWORDS: *electrospinning, carbon nanofiber, lithium ion battery, nickel, SnO_2 stabilization*

INTRODUCTION

Lithium ion batteries (LIBs) are attractive power sources for a wide range of mobile devices such as smart phones, laptop computers, and hybrid electric vehicles. There have been tremendous interests in developing novel nanomaterials for advanced LIB electrodes, particularly to improve the energy capacity and cycling stability.[1,2] Selected metals that can alloy with lithium, such as Si, Ge, and Sn, are considered to be promising alternatives to the graphite anode currently used in Li-ion batteries with a relatively low theoretical capacity of 372 mA h g^{-1}.[3,4] Sn has attracted intensive research interest as a next generation anode material because of its high theoretical capacity (990 mA h g^{-1}).[5] However, Sn anodes have a fatal drawback because of the large volume expansion that accompanies the lithium–dealloying process.[6] This volume expansion results in severe mechanical strain, which often leads to pulverization of the lithium–alloy particles ($Li_{4.4}Sn$) and poor cyclability.[7]

One of the possible approaches to overcoming the pulverization issue is to use nanostructured electrodes. One-dimensional nanostructured electrodes show better performance than their macrostructured counterparts, due to the reduced diffusion length and alleviated mechanical stress during the charging/discharging cycles.[8] However, their high synthesis costs, as well as the present technological limitations, make the use of Sn nanowires/nanotubes difficult. One other possible strategy is to use a composite of Sn-carbon materials, which is a synergistic combination resulting in both high capacity and good cyclability.[9] A wide variety of carbon materials, such as carbon nanofibers (CNFs), carbon nanotubes, and graphene, have been applied as either a matrix or surface coating for accommodating volume change and preventing aggregation.[10−13] Among them, CNFs are inexpensive and can be produced with various controlled structures at relatively high rates.[14] Recently, the electrospinning technique has been used to fabricate composite anode materials consisting of Sn/SnO_2 nanoparticles and CNFs.[15] The electrochemical performance of the electrospun Sn/SnO_2–CNFs composite can be improved

Received: July 13, 2012
Accepted: September 21, 2012
Published: September 21, 2012

by introducing pores with the aid of either a template or phase separation in which the Sn/SnO_2 nanoparticles stably reside.[16] Porous CNFs can prevent the segregation of Sn agglomerates upon melting (the melting point of Sn = 210 °C), so that size distribution of pores should be carefully controlled to disperse Sn/SnO_2 nanosized particles.

The electrospun polymeric nanofibers containing Sn salts undergo stabilization in air at 250 °C, followed by carbonization in an inert atmosphere at 600−800 °C. The Sn salt is decomposed and subsequently formed to SnO_2 in the form of nanoparticles attached to the carbon fibers. The carbonization temperature should be maintained as high as 800 °C. Otherwise, SnO_2 is reduced to metallic Sn through carbothermal reduction during carbonization.[17,18] The metallic Sn is thermodynamically incompatible with the carbon system such that it is readily segregated into large agglomerates on the surface of the CNFs by melting. The thermal instability of Sn can be improved by forming intermetallic binary alloy compounds, M_xSn_y (M = Cu, Ni, Co, Sb, Ag, Fe).[19,20] Ni_xSn_y alloy systems can also alleviate, to some extent, the large volume changes that occur during the insertion and extraction processes.[21] From this perspective, electrospun intermetallic Ni_xSn_y compound-embedded carbon nanofiber composites were reported.[22] However, the Ni−Sn alloy has relatively low capacity (580 mA h g^{-1} for Ni_3Sn_2), and the carbonization at lower temperature prevents the production of high-quality CNFs with good electrical conductivity for efficient charge transport.[23]

In this study, we synthesized an electrospinning-derived Ni added SnO_2−CNF composite as a promising anode material with a high specific capacity and excellent cycle retention. To improve the thermal stability of Sn−C, light Ni addition was introduced without forming a bimetallic alloy. The presence of the Ni enhanced the adhesion characteristics of Ni−C and Ni−Sn such that the SnO_2/NiO nanoparticles were firmly adhered to both the inner and outer surfaces of the CNFs, even when the polymeric nanofibers were carbonized at high temperature enough to maximize the electrical conductivity of the CNF matrix. We investigated the influence of the Ni adding concentration on the morphology and the phase of the Ni-added SnO_2−CNF composites as well as their electrochemical properties.

EXPERIMENTAL METHOD

Synthesis of Metal/Metal Oxide−CNF Composites. To prepare the precursor solution for electrospinning, polyacrylonitrile (PAN, M_w = 150 000, Aldrich) was dissolved in dimethylformamide (DMF, anhydrous, 99.8%, Aldrich) by stirring in a 20 mL vial at 60 °C for 24 h. Tin chloride dehydrate (Aldrich) and/or nickel chloride hydrate (Aldrich) were added to the prepared solution and then vigorously stirred at room temperature until a homogeneous solution was obtained. The amount of metal salt(s) added to the PAN was 30 wt %, and several solutions with varying compositions were prepared using pure Sn, Sn:Ni = 95:5 wt %, 90:10 wt %, and 80:20 wt % (denoted as PAN/Ni0%, PAN/Ni5%, PAN/Ni10%, and PAN/Ni20%). The composition represented the weight % of the metallic phases, assuming that all of the metal salts were converted to metal particles. The viscosity of the polymer solutions was in the range of 1000−1200 mPa s, as determined by a rheometer (AR-2000EX, TA Instruments). The polymer−metal salt(s) solutions were electrospun through a stainless steel nozzle (inner diameter = 0.21 mm) by applying a voltage of 9 kV using a high-voltage DC power supply unit (Nanotech) at a distance of 15 cm between the nozzle tip and the drum collector. The polymer−metal salt(s) solution was supplied by a syringe pump (KD100, KD Scientific) at a flow rate of 0.1 mL h^{-1}. As-electrospun composite polymer fibers were dried at 80 °C for 24 h, followed by stabilization at 250 °C for 8 h in air, and then carbonization was performed at 900 °C for 2 h in an argon atmosphere at a rate of 5 °C min^{-1}. To determine the effect of the carbonization temperature, the CNF/Ni10% samples were carbonized at various temperatures ranging from 700 to 1000 °C.

Structural Analyses of Metal/Metal Oxide−CNF Composites. Structural characterization of the nanofibers was performed using an X-ray diffractometer (XRD, D/max 2500H, Rigaku co., Cu Kα, λ=0.154 nm) at 40 kV and 200 mA. The thermal decomposition behavior of the electrospun composite carbon fibers was determined using a thermal gravimetric-differential scanning calorimeter (TG-DSC, Q600, TA Instruments) in either an argon or air atmosphere. The morphologies of the carbonized composite fibers were monitored by a field emission scanning electron microscope (FE-SEM, JSM-6700F, JEOL) and a transmission electron microscope (TEM, JEM-2100F, JEOL). The surface chemical structures of the composite carbon fibers were analyzed by X-ray photoelectric spectroscopy (XPS, ESCALAB 220i-XL, VG Scientific).

Electrochemical Characterization of Metal/Metal Oxide−CNF Composites. The electrochemical performance was assessed using a CR2032 coin type half-cell. A metallic lithium sheet was used as the reference and counter electrodes with a micro porous polymer separator (Celgard2325, Celgard Korea) and liquid electrolyte mixtures containing 1 mol L^{-1} $LiPF_6$ and a solvent mixture of ethylene carbonate (EC) and diethylcarbonate (DEC) (1:1 by volume) (Chameleon Reagents, Japan). The testing electrodes were prepared by coating the slurry onto a copper foil, which consisted of carbon fiber nanocomposites, polyvinylidenefluoride (PVDF, Aldrich), and super P (conductive carbon black, Alfa Aeser) at a weight ratio of 80:10:10. After drying in a vacuum oven at 100 °C, the electrodes were punched into a circle and assembled in the cell in a glovebox (Super-1220, Mikrouna) filled with pure argon. The voltage profile curves were measured at the potential range of 0.01−1.5 V vs Li/Li^+ at 200 mA g^{-1}, and galvanostatic discharge (Li^+ insertion) and charge (Li^+ extraction) were performed with the voltage between 0.01 and 1.5 V vs Li/Li^+ at a current density of 50 mA g^{-1} using a battery testing system (Neware Electronic Co., China).

RESULTS AND DISCUSSION

The metal/metal oxide nanoparticles-embedded CNFs were prepared by electrospinning the precursor solutions, followed by carbonization at 900 °C for 2 h in an argon atmosphere. Four different precursor solutions were used in which the metallic compositions included pure Sn, Ni:Sn = 5:95, 10:90, and 20:80 wt %. The resulting CNF composites were denoted as CNF/Ni0%, CNF/Ni5%, CNF/Ni10%, and CNF/Ni20%, respectively. As electrospun polyacrylonitrile (PAN) composites after stabilization at 250 °C in air showed a continuous and uniform fibrous morphology without beads, regardless of the composition (see the Supporting Information, Figure S1). The diameter of the nanofibers was in the range of 300−400 nm, and the surface was smooth and free of segregated metal salt particles. Figure S2a in the Supporting Information shows the thermal decomposition behavior of the electrospun PAN/Ni10% fiber under an argon atmosphere. An abrupt weight loss (12 wt %) occurred, accompanying an exothermic peak in the vicinity of 210−250 °C, followed by a gradual weight loss. The exothermic reaction at 210−250 °C can be ascribed to the cyclization reaction of the nitrile groups. The difference in the remnant weights after carbonization under Ar and air allowed us to determine the carbon−metallic phase composition (see the Supporting Information, Figure S2b). The Ni(II) chloride and Sn(II) chloride-embedded PAN nanofibers were pyrolyzed in air at 900 °C where all of the carbon species were eliminated, leaving behind the oxidized Ni and Sn. Assuming that the remaining phases were NiO and SnO_2, we determined the

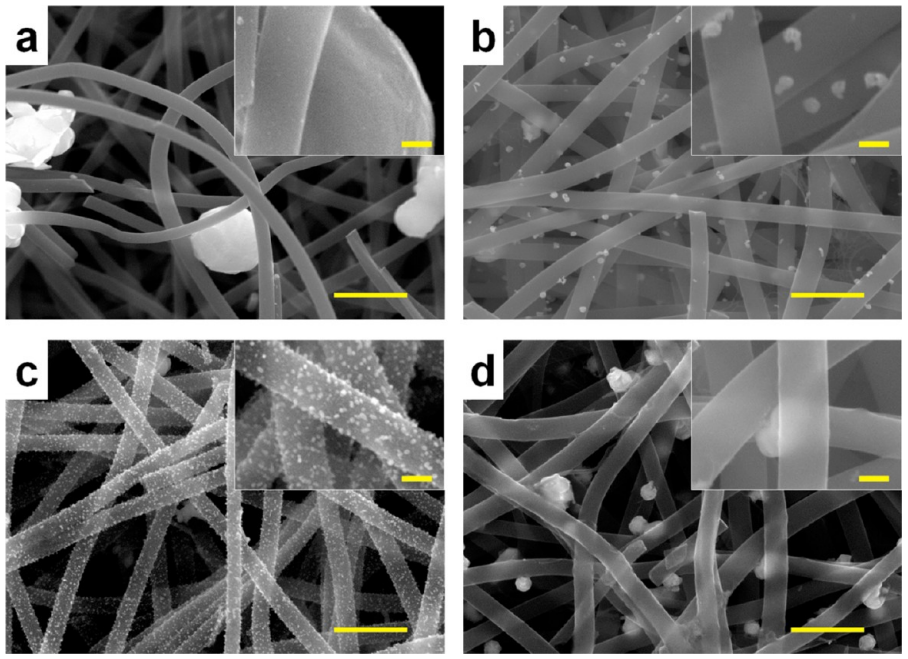

Figure 1. SEM images of (a) CNF/Ni0%, (b) CNF/Ni5%, (c) CNF/Ni10%, and (d) CNF/Ni20% carbonized at 900 °C. The scale bars in the figures and insets represent 1 μm and 100 nm, respectively.

composition of the metallic phase-CNFs composite after carbonization to carbon:metal oxides ($NiO+SnO_2$) = 77.3:22.7 wt % based on multiple measurements.

Figure 1 shows the morphology of the as-synthesized metal/metal oxide-CNF composites. The fibers shrank during carbonization to a diameter of 170 ± 30 nm, and substantial differences in the surface morphologies were observed, depending upon the carbon-to-metal ratio. It was easy to distinguish the metal and/or metal oxide from the CNFs because of the differences in brightness. For CNF/Ni0%, continuous fibers with smooth surfaces were observed, with occasional large particles of 1 μm located separately from the CNTs (Figure 1a). In contrast, the addition of Ni noticeably altered the morphology of the CNF composites (Figure 1b–d). A few particles that were 50 nm in size were attached to the carbon fibers in the 5% Ni-added Sn-CNFs (Figure 1b). Many smaller particles that were 15 nm in size were uniformly distributed around the CNFs when 10 wt % of Sn was replaced by Ni (Figure 1c). Further addition of Ni at 20 wt % resulted in the recurrence of large particles that were 150 nm in size scattered between the smooth CNFs (Figure 1d). The compositional distribution in the metal-CNF composites was determined by energy-dispersive X-ray spectroscopy (EDX). The large bright particles in the CNF/Ni0% sample were composed of either Sn and O or Sn only, indicative of a mixture of tin oxide and Sn (see the Supporting Information, Figure S3). On the other hand, Sn, Ni, and O elements were well-dispersed on the CNF surface in the case of CNF/Ni10%, implying that the tin oxide/nickel oxide nanoparticles were uniformly distributed on the CNFs (see the Supporting Information, Figure S4). In contrast, the CNF/Ni20% contained large particles supporting the coexistence of Sn, Ni, and O or Sn and Ni with oxygen (see the Supporting Information, Figure S5), indicative of a mixture of a bimetallic phase and an oxidized metallic phase.

Figure 2 shows the X-ray diffraction (XRD) patterns of the metal/metal oxide-CNF composites as a function of the

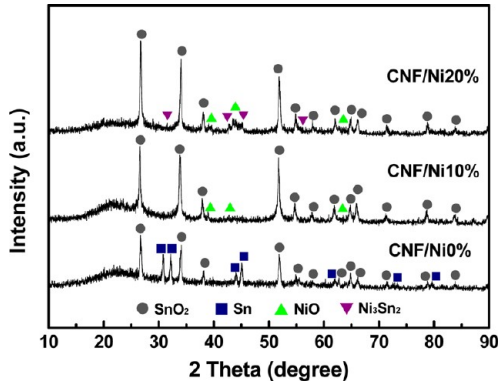

Figure 2. X-ray diffraction (XRD) patterns of carbonized CNF/Ni0% (bottom line), CNF/Ni10% (center line), and CNF/Ni20% (top line).

metallic phase compositions. All of the samples exhibited a broad peak of amorphous graphitic carbon near 25°. The CNF/Ni0% sample had two characteristic diffraction peaks that can be attributed to the SnO_2 tetragonal rutile structure (JCPDS 88–0287) and metallic Sn (JCPDS 04–0673). This means that Sn^{2+} can be transformed to metallic Sn through carbothermal reduction during carbonization at high temperature.[19,20] Tin dioxide peaks were detected at 26.59, 33.87, and 51.78°, which can be ascribed to the (110), (101), and (211) planes, respectively. Metallic Sn peaks were also observed at 30.64, 32.02, and 43.87°, which correspond to the (200), (101) and (220) planes, respectively.[19] In contrast, the crystalline oxide phases of SnO_2 and NiO appeared in CNF/Ni10% and CNF/Ni20% without metallic Sn. Both CNF/Ni10% and CNF/Ni20% had strong peaks corresponding to SnO_2 where the (110), (101), and (211) planes were observed, while relatively weak peaks of nickel oxide were detected at 37.48, 42.83, and 62.87°, corresponding to the (111), (200), and (220) planes, respectively.[24] The low intensity of the NiO peaks resulted

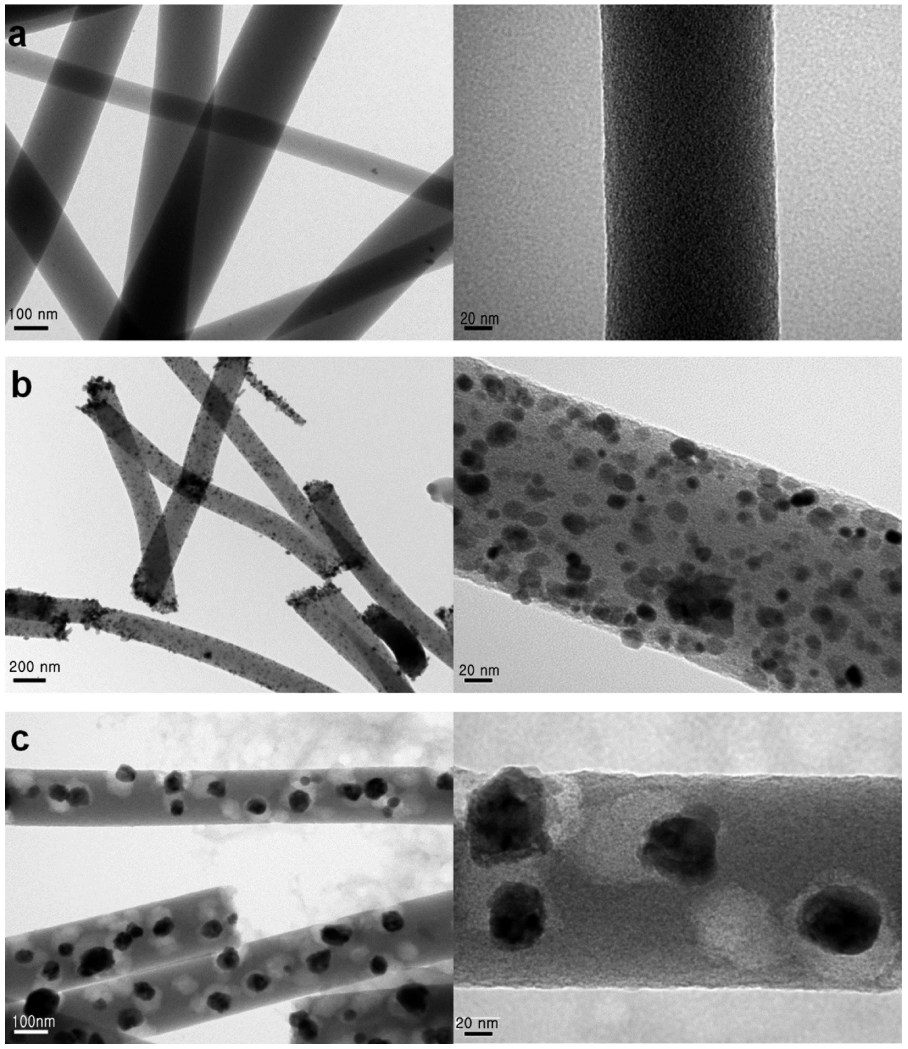

Figure 3. TEM images of (a) CNF/Ni0%, (b) CNF/Ni10%, and (c) CNF/Ni20% carbonized at 900 °C. The CNF/Ni0% sample had few particles on the CNF surface, but the CNF/Ni10% sample showed nanoparticles smaller than 20 nm attached to the CNF surface as well as located inside of CNF. The CNF/Ni20% had much larger particles of 150 nm.

from its scarcity. In the case of CNF/Ni20%, a Ni−Sn alloy formed under the Ni-rich conditions. A Ni_3Sn_2 alloy (JCPDS 06−0414) was detected at 30.80, 43.58, 44.50, and 55.10°, corresponding to the (101), (102), (110), and (112) planes, respectively.

Detailed microstructures of the synthesized metal/metal oxide-CNF composites were examined by transmission electron microscopy (TEM) as shown in Figure 3. Two different sized particulate phases were detected in the CNF/Ni0% sample. The particles were mostly located at both the inner and outer surfaces of the carbon nanofibers, on which few nanosized particles were attached (Figure 3a), whereas the large particles (not seen in Figure 3a) appeared to be separated from the carbon nanofibers. As mentioned previously, the huge particles with sizes of 1 μm were composed of Sn/SnO_2, according to the SEM and EDX analyses. The CNF/Ni10% sample had more particles that were 15 nm in size. These nanoparticles consisted of NiO and SnO_2, both of which were homogeneously located on the surfaces of the CNFs according to the EDX and TEM results (Figure 3b and Figure S4 in the Supporting Information). Likewise, Figure 3c shows a TEM image of the CNF/Ni20% sample, where more grown particles that were 150 nm in size were embedded in the CNFs. These large particles would reduce the capacity during Li^+ insertion/extraction. However, small particles dispersed on the surfaces of the CNFs, as seen in the CNF/Ni10% sample, can tolerate the damage induced by the volume change during lithiation. Thus, 10 wt % Ni was the optimum addition amount when carbonized at 900 °C.

Figure 4 shows the X-ray photoelectric spectroscopy (XPS) analysis of the metal-CNF composites. The carbon 1s spectrum at ~284.5 eV was used as a reference for calibration. For CNF/Ni0%, the Sn $3d_{5/2}$ spectrum was decomposed to subpeaks with binding energies (BE) of 486.1 and 486.7 eV, which were assigned to the metallic Sn^o state and Sn^{4+} state in SnO_2, respectively (Figure 4a).[25] These XPS results support the coexistence of metallic Sn and SnO_2 in the absence of Ni, which is consistent with the XRD results. In contrast, variations in the Sn $3d_{5/2}$ spectra were observed as a function of the Ni content when nickel was added to the CNFs. CNF/Ni10% showed the Sn^{4+} state (BE of 486.9 eV), which was attributed to only SnO_2 (Figure 4b). No metallic state of Sn^o (BE of 486.1 eV) was observed. This supports the fact that both samples had the same SnO_2 phase, and also that the additional metallic state of Sn^o needs to be exactly deconvoluted. CNF/Ni20% had totally different spectra than the others. The Sn^{4+} state with a BE of

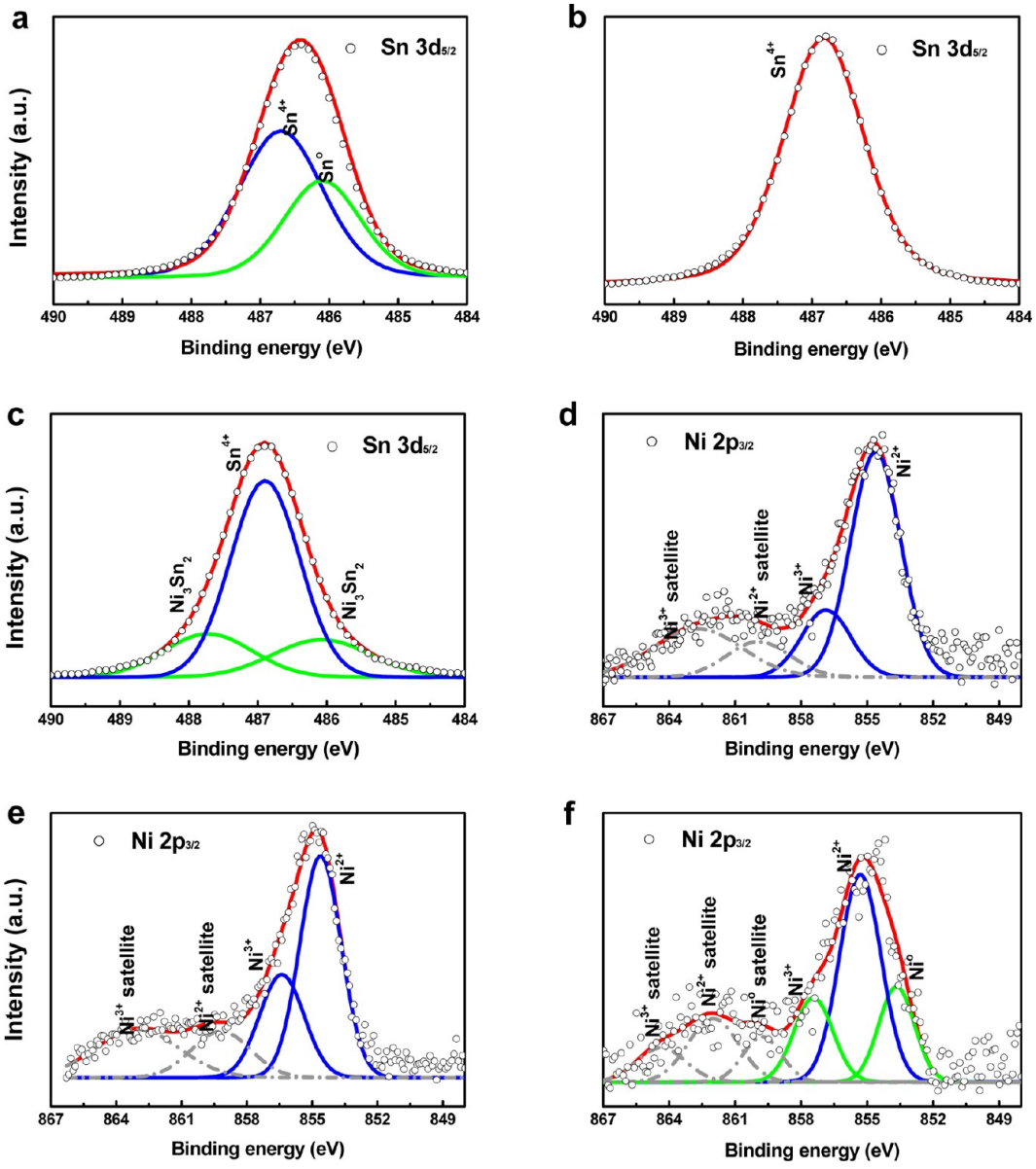

Figure 4. XPS spectra of CNF/Ni0%, CNF/Ni5%, CNF/Ni10%, and CNF/Ni20% carbonized at 900 °C. Sn peak of (a) CNF/Ni0%, (b) CNF/Ni10%, and (c) CNF/Ni20%. Ni $2p_{3/2}$ of (d) CNF/Ni5%, (e) CNF/Ni10%, and (f) CNF/Ni20%.

486.1 eV and minor states of 486.2 and 487.7 eV were observed, which were assigned to the intermetallic state of Ni_3Sn_2 (Figure 4c). The grown particles observed in the SEM analysis might be due to this intermetallic state.

Like the Sn $3d_{5/2}$ spectra, the Ni $2p_{3/2}$ spectra showed a similar tendency depending on the Ni composition. Generally, the Ni $2p_{3/2}$ spectra of oxides and other compounds are interpreted on the basis of the main peak (at 854.6 eV) and the broad satellite (centered at ~861 eV in NiO).[26] Panels d and e in Figure 4 show the Ni states of CNF/Ni5% and CNF/Ni10%, respectively. Both samples had two main states at BEs of 854.7 and 856.3 eV, which are assigned to Ni^{2+} and Ni^{3+}, respectively. Only the nickel oxide phase existed without the metallic Ni phase. The NiO phase (at 854.5 eV of Ni^{2+}) and the Ni_3Sn_2 alloying phase were observed in the spectrum of the CNF/Ni20% sample (Figure 4f). Intermetallic Ni_3Sn_2 had BEs of 852.9 and 856.1 eV, which were indicative of a metallic Ni state.[22] The presence of the intermetallic state of Ni_3Sn_2 was confirmed by SEM-EDX and Sn $3d_{5/2}$ spectra analyses. The Ni-rich composition likely induced the alloying of Ni and Sn. Table 1 summarizes the XPS results in terms of the binding energy and phase for the carbonized metallic phase-CNF composites.

On the basis of our SEM and XPS analyses, it can be inferred that Sn is thermodynamically unstable in a carbon matrix. The SnO_2 phase in a carbon matrix is likely reduced to metal by carbothermal reduction, which is separated from the CNFs as huge agglomerates upon its melting. When Sn is added to CNFs in the form of salts such as tin chloride, the Sn might be converted to SnO_2 during the stabilization process of CNFs in air at 250 °C. Carbothermal reduction readily occurs above 550 °C.[17,18] Although the detailed mechanism of carbothermal reduction is not clearly understood, the bond strength of C−O (1076.5 ± 0.4 kJ mol^{-1}, calculated from the diatomic gaseous state) is much stronger than that of Sn−O (531.8 ± 12.6 kJ mol^{-1}).[27] The thermally activated reduction of SnO_2 is unavoidable, but could be retarded by the addition of Ni. The stabilization of SnO_2 by Ni addition has been researched in

dx.doi.org/10.1021/am301328u | ACS Appl. Mater. Interfaces 2012, 4, 5408−5415

Table 1. Analysis of XPS Spectra and Phase Assignment

sample	binding energy (eV)		fwhm (eV)	phase assignment
CNF/Ni0%	Sn $3d_{5/2}$	486.1	1.29	Sn
		486.7	1.44	SnO_2
CNF/Ni5%	Ni $2P_{3/2}$	854.6, 856.9	1.88, 1.64	NiO
	Sn $3d_{5/2}$	486.8	1.38	SnO_2
CNF/Ni10%	Ni $2P_{3/2}$	854.7, 856.3	1.84, 1.27	NiO
	Sn $3d_{5/2}$	486.9	1.44	SnO_2
CNF/Ni20%	Ni $2P_{3/2}$	854.5	1.88	NiO
		852.9, 856.1	1.46, 1.53	Ni_3Sn_2
	Sn $3d_{5/2}$	486.9	1.44	SnO_2
		486.2, 487.7,	1.72, 1.68	Ni_3Sn_2

the development of SnO_2 sensors. Ni can be located easily in the lattice sites of SnO_2 in the form of NiO due to the similar ionic radii of Ni^{2+} and Sn^{4+}, or in the surface sites forming a stable p(NiO)-n(SnO_2) junction, which increases the thermal stability of SnO_2.[28,29] Stabilization of SnO_2 can prevent it from reducing to Sn, which will in turn transform into large agglomerates that are separated from the CNFs upon melting. This concept is also indirectly supported by the decoking phenomena of Ni anodes in solid oxide fuel cells; carbon deposition easily occurs when using Ni catalysts over which hydrocarbon fuel is oxidized. Nikolla et al. demonstrated a solution to the carbon coking problem by Sn doping of Ni catalysts. Doped Sn at the surface is readily alloyed with Ni, enhancing the cleavage of C−C bonding and in turn inhibiting the generation of coke.[30−33] In other words, Sn and C are thermodynamically unstable, but Ni is stable with both Sn and C, as characterized by the preferential Sn−Ni alloying and easy carbon deposition on Ni. In this respect, the addition of Ni to SnO_2−CNF enables SnO_2 to reside stably with the carbon matrix.

Figure 5 shows the electrochemical performance of the cells with SnO_2/CNF and Ni-added SnO_2/CNF composite anodes. From the TGA data (see the Supporting Information, Figure S2), the theoretical specific capacity of the composite was calculated to be 491.5 mA h g^{-1} based on the reversible capacities of the CNF (372 mA h g^{-1}) and SnO_2 (780 mA h g^{-1}), where the weight fraction of CNF:SnO_2 was 0.7072:0.2928. NiO is inert to Li ion insertion commonly operated at charge/discharge potential from 0.1 to 1.5 V. All samples delivered high Li^+ storage and a large initial capacity of current density at 200 mA g^{-1} as shown in Figure 5a. The rapid degradation of the initial capacity indicates the irreversibility resulting from the formation of a solid electrolyte interface (SEI) layer. The SEI layer, which is generated on the carbon and SnO_2 in the form of Li_2O, is an electron insulator, thereby disturbing the electron transfer.[34,35] Cyclic voltammetry showed that the SEI formation occurred only at the first cycle, as indicated by a reduction peak near 0.90 V (vs Li/Li^+) during the first cycle (see the Supporting Information, Figure S6).[34] The further decrease in the capacity is attributed to the pulverization of SnO_2 caused by the drastic volumetric change of the SnO_2 during the insertion and extraction of the Li^+ ions. Well-dispersed nanosized and stabilized SnO_2 particles were well-attached onto the CNFs, which avoid pulverization due to the minimized volumetric change in the nanoscale particles. In this respect, CNF/Ni10% had the optimum morphology, so it

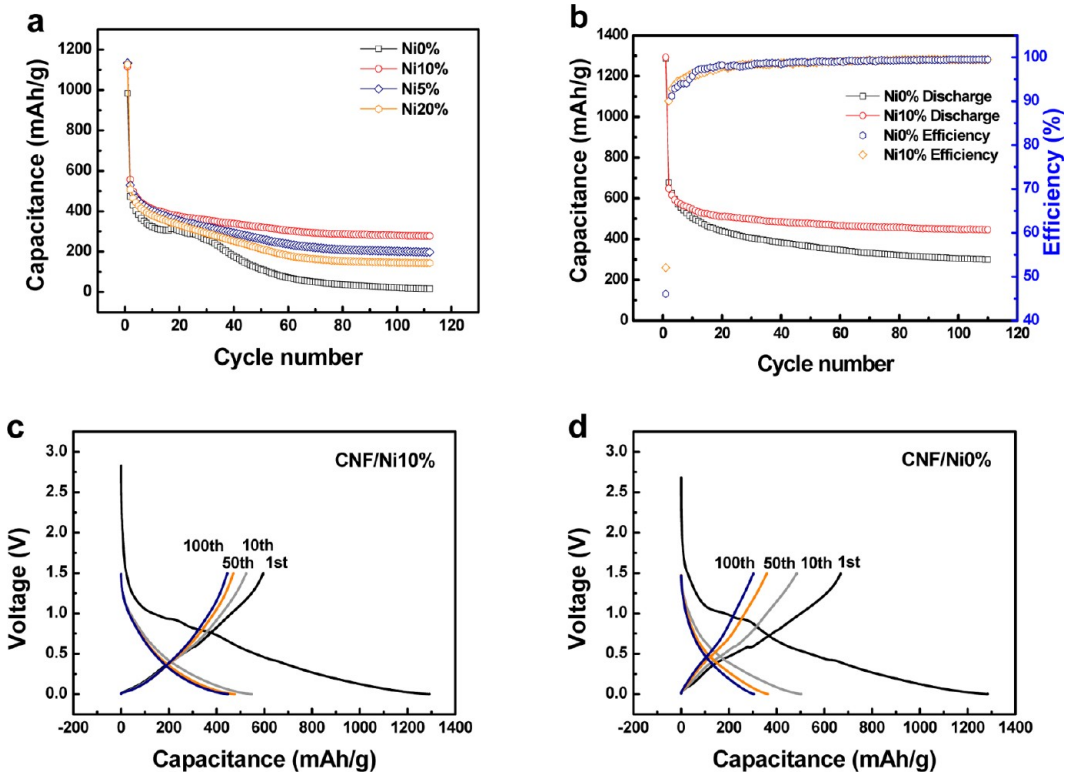

Figure 5. Electrochemical performance of CNF/Ni0%, CNF/Ni5%, CNF/Ni10%, and CNF/Ni20% carbonized at 900 °C. (a) Discharge capacity of all samples at a current density of 200 mA g^{-1}. (b) Discharge/charge curves and Coulombic efficiency versus cycle number for CNF/Ni0% and CNF/Ni10% at a current density of 50 mA g^{-1}. Voltage profiles of (c) CNF/Ni10% and (d) CNF/Ni0% electrodes in half cells cycled between 20 mV and 1.5 V at a current density of 50 mA g^{-1}.

dx.doi.org/10.1021/am301328u | ACS Appl. Mater. Interfaces 2012, 4, 5408−5415

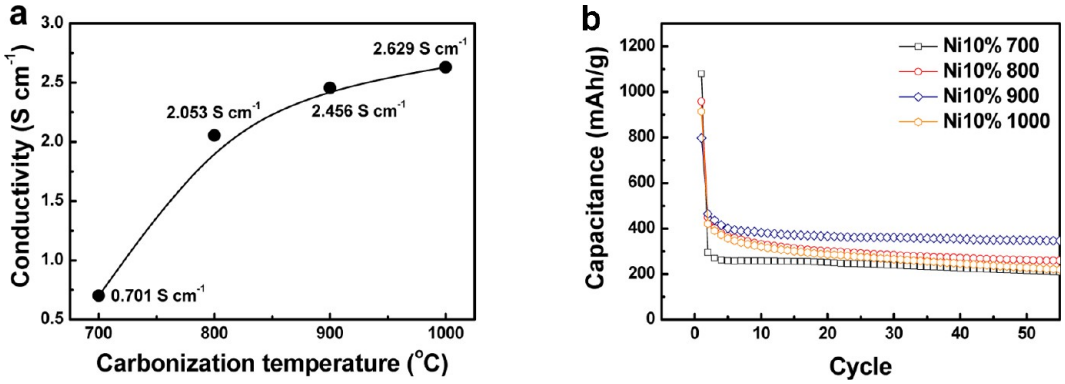

Figure 6. (a) Electrical conductivities and (b) discharge capacities of CNF/Ni10% at a current density of 200 mA g^{-1}. The carbonization temperature of the CNFs was varied from 700 to 1000 °C.

exhibited the best cycle stability. Both the CNFs mixed with 5% and 20% Ni also showed better cycling performance than CNF/Ni0. However, the CNF/Ni20% sample had lower reversible capacity than the CNF/Ni10% because of large agglomerates of SnO_2 particles. Well-dispersed fine SnO_2 particle formation, assisted by enhanced compatibility with the carbon, led to less degradation and better stability during the Li insertion/extraction.

For a more accurate analysis of the Ni addition influence, the cycling performance of CNF/Ni0% and CNF/Ni10% at 50 mA g^{-1} was compared as shown in Figure 5b. Although both of the samples showed Coulombic efficiencies higher than 99.2% after the fifth cycle, the capacity of Ni0% still continued to diminish, with a capacity of 304.6 mA h g^{-1} after 100 cycles, while that of Ni10% remained constant at a capacity of 447.6 mA h g^{-1}. Considering the fact that the SnO_2 was only 29.28% of the anode weight, the capacity of 447.6 mA h g^{-1} was relatively high compared to its calculated theoretical specific capacity of 491.5 mA h g^{-1}. Although both CNF/Ni0% and CNF/Ni10% had high Coulombic efficiency, more than half of their initial capacity was lost after 100 cycles. As seen in the voltage profiles of CNF/Ni10% and CNF/Ni0% in Figure 5c, d, no remarkable change in the charge/discharge profile was observed after 100 cycles for CNF/Ni10%, indicating stable cycling performance due to the controlled volume expansion and pulverization of well-dispersed nanosized SnO_2 (Figure 5c). In contrast, the voltage profile of CNF/Ni0% (without a Ni component) revealed continuous capacity degradation (Figure 5d). Our CNF/Ni10% had not only the appropriate morphology, but also the highest specific capacity and the best cycling performance among the anodes to which Ni was added.

The influence of Ni on the stabilization of the SnO_2-carbon system would differ as a function of the carbonization temperature. All of the previous studies of electrospun Sn/CNF anodes involve the maximum carbonization of 700 °C.[16−18] A higher carbonization temperature could give rise to higher electrical conductivity of the CNFs, such that carbonization at temperatures above 700 °C would enable higher performance of the anodes. We performed the cycling test of CNF/Ni10% carbonized at varying temperatures from 700 to 1000 °C (Figure 6a). The electrical conductivity increased with increasing carbonization temperature. The improved electrical conductivity likely resulted from the effective removal of hydrogen and oxygen, as well as the enhanced crystallization of graphitic carbon. The CNFs acted not only as a buffering agent against volume expansion and pulverization of metal oxide or metallic particles but also as an electrical conductor to facilitate electron transfer. Figure 6b shows the electrochemical performance of CNF/Ni10% with varying carbonization temperatures at a current density of 200 mA g^{-1}. As expected, the CNF/Ni10% carbonized at 700 °C showed the lowest discharge capacity of 215.2 mAh g^{-1}, and the cell carbonized at 800 °C exhibited a capacity of 262.7 mAh g^{-1} after 50 cycles. With the decreased electric conductivity of the CNFs, the charge potential distribution becomes less uniform within the electrode, which leads to a decrease in the discharge capacity.[23] The CNF/Ni10% carbonized at 900 °C demonstrated the highest discharge capacity of 349.3 mAh g^{-1} and excellent capacity retention during 50 cycles. Because the metal loading in the CNF was identical, the higher performance of the cells carbonized at higher temperatures was attributed to more effective electron transfer through the CNFs. In contrast, the CNF/Ni10% carbonized at 1000 °C showed lower capacity (215.2 mAh g^{-1}) than the one carbonized at 900 °C with a continuous decrease in the capacity. Although Ni was added to stabilize the SnO_2, huge agglomerates were observed as shown in Figure S7 (in the Supporting Information), which presumably accelerated pulverization of the anodes.

CONCLUSIONS

We synthesized SnO_2−NiO/CNF nanocomposite fibers by electrospinning. Addition with a small amount of Ni alleviates the pulverization and capacity fading of the SnO_2 loaded on the electrospun CNFs. Thermally activated reduction of SnO_2 is unavoidable during the carbonization of polymer nanofibers containing metal salt, leading to the formation of large agglomerates that are segregated from the CNFs, which in turn induce capacity fading during the charge/discharge cycles. Ni can be located easily in the lattice sites of SnO_2 in the form of NiO, through which the thermal stability of SnO_2 improves. The stabilization of the nanosized SnO_2 particles then prevents them from being reduced to Sn, which is subjected to melting, subsequently forming large agglomerates. It was confirmed by SEM and TEM that Ni presence stabilizes SnO_2 on CNFs in that 15 nm SnO_2 nanoparticles were uniformly distributed onto the CNFs, while huge agglomerates of 1 μm appeared in the absence of Ni. Our simple approach of Ni addition successfully resolved the problems associated with the reduction/aggregation of SnO_2 when carbonized at temperatures above 800 °C and the pulverization of SnO_2 during battery operation. All of the Ni-added SnO_2/CNF composite anodes exhibited better morphology after carbonization at 900 °C and better

cyclability during the charge/discharge test compared to the Sn-SnO_2/CNFs without Ni. Among them, the CNF/Ni10% carbonized at 900 °C demonstrated the highest specific capacity retention of 447.6 mA h g^{-1} after 100 cycles, whereas the CNF/Ni0% showed a capacity retention of 304.6 mA h g^{-1} at 50 mA g^{-1}.

■ ASSOCIATED CONTENT

Supporting Information

SEM images of the polymer fibers as function of Ni content, TGA analysis, EDX mapping images, cyclic voltammograms, FE-SEM image of 1000 °C carbonized fibers. This material is available free of charge via the Internet at http://pubs.acs.org.

■ AUTHOR INFORMATION

Corresponding Author

*Tel.: +82 2 2123 2855. Fax: +82 2 312 5375. E-mail: jmoon@yonsei.ac.kr; joosun@kist.re.kr.

Notes

The authors declare no competing financial interest.

■ ACKNOWLEDGMENTS

This work was supported by a grant from the National Research Foundation of Korea funded by the Korean government (MEST) (NRF-2010-0028971 and 2012R1A3A2026417). It was also partly supported by the Second Stage of the Brain Korea 21 Project.

■ REFERENCES

(1) Bruce, P. G.; Scrosati, B.; Tarascon, J.-M. *Angew. Chem., Int. Ed.* **2008**, *47*, 2930−2946.
(2) Guo, Y.-G.; Hu, J.-S.; Wan, L.-J. *Adv. Mater.* **2008**, *20*, 2878−2887.
(3) Zhang, W.-M.; Hu, J.-S.; Guo, Y.-G.; Zheng, S.-F.; Zhong, L.-S.; Song, W.-G.; Wan, L.-J. *Adv. Mater.* **2008**, *20*, 1160.
(4) Chan, C. K.; Patel, R. N.; O'Connell, M. J.; Korgel, B. A.; Cui, Y. *ACS Nano* **2010**, *4*, 1443.
(5) Lee, K. T.; Jung, Y. S.; Oh, S. M. *J. Am. Chem. Soc.* **2003**, *125*, 5652.
(6) Yu, Y.; Gu, L.; Wang, C.; Dhanabalan, A.; van Aken, P. A.; Maier, J. *Angew. Chem. Inter. Edi.* **2009**, *48*, 6485.
(7) Noh, M.; Kwon, Y.; Lee, H.; Cho, J.; Kim, Y.; Kim, M. G. *Chem. Mater.* **2005**, *17*, 1926−1929.
(8) Kim, M. G.; Cho, J. *Adv. Funct. Mater.* **2009**, *19*, 1497.
(9) Derrien, G.; Hassoun, J.; Panero, S.; Scrosati, B. *Adv. Mater.* **2007**, *19*, 2336.
(10) Liu, B.; Guo, Z. P.; Du, G.; Nuli, Y.; Hassan, M. F.; Jia, D. *J. Power Sources* **2010**, *195*, 5382.
(11) Xing, L.-L.; Ma, C.-H.; Cui, C.-X.; Xue, X.-Y. *Solid State Sci.* **2012**, *14*, 111.
(12) Li, Y.; Zhu, S.; Liu, Q.; Gu, J.; Guo, Z.; Chen, Z.; Feng, C.; Zhang, D.; Moon, W.-J. *J. Mater. Chem.* **2012**, *22*, 2766−2733.
(13) Wang, H.; Gao, P.; Lu, S.; Liu, H.; Yang, G.; Pinto, J.; Jiang, X. *Electrochim. Acta* **2011**, *58*, 44.
(14) Yu, Y.; Gu, L.; Zhu, C.; van Aken, P. A.; Maier, J. *J. Am. Chem. Soc.* **2009**, *131*, 15984.
(15) Yang, Z.; Du, G.; Guo, Z.; Yu, X.; Chen, Z.; Zhang, P.; Chen, G.; Liu, H. *J. Mater. Res.* **2010**, *25*, 1516.
(16) Zou, L.; Gan, L.; Lv, R.; Wang, M.; Huang, Z.-H.; Kang, F.; Shen, W. *Carbon* **2011**, *49*, 89.
(17) Yu, Y.; Yang, Q.; Teng, D.; Yang, X.; Ryu, S. *Electrochem. Commun.* **2010**, *12*, 1187.
(18) Yang, S.; Song, H.; Chen, X. *J. Power Sources* **2007**, *173*, 487.
(19) Li, H.; Shi, L.; Wang, Q.; Chen, L.; Huang, X. *Solid State Ionics* **2002**, *148*, 247.
(20) Mukaibo, H.; Sumi, T.; Yokoshima, T.; Momma, T.; Osaka, T. *Electrochem.Solid-State Lett.* **2003**, *6*, A218.
(21) Hassoun, J.; Panero, S.; Simon, P.; Taberna, P. L.; Scrosati, B. *Adv. Mater.* **2007**, *19*, 1632.
(22) Jung, H.-R.; Lee, W.-J. *J. Electrochem. Soc.* **2011**, *158*, A644.
(23) Lee, Z. K.; An, K. W.; Ju, J. B.; Cho, B. W.; Cho, W. I.; Park, D.; Yun, K. S. *Carbon* **2001**, *39*, 1299−1305.
(24) Song, G; Han, J.; Guo, R. *Synth. Met.* **2007**, *157*, 170.
(25) Jie, L.; Chao, X. *J. Non-Cryst. Solids* **1990**, *119*, 37.
(26) Onda, A.; Komatsu, T.; Yashima, T. *Phys. Chem. Chem. Phys.* **2000**, *2*, 2999.
(27) Kerr, J. A. *CRC Handbook of Chemistry and Physics 1999−2000: A Ready-Reference Book of Chemical and Physical Data (CRC Handbook of Chemistry and Physics*, 81st ed.; Lide, D.R., Ed.; CRC Press: Boca Raton, FL, 2000.
(28) Yang, G.; Haibo, Z.; Biying, Z. *J. Mater. Sci.* **2000**, *35*, 917.
(29) Hidalgo, P.; Castro, R. H. R.; Coelho, A. C. V.; Gouvêa, D. *Chem. Mater.* **2005**, *17*, 4149.
(30) Koh, J.-H.; Kang, B.-S.; Lim, H. C.; Yoo, Y.-S. *Electrochem. Solid-State Lett.* **2001**, *4*, A12.
(31) Koh, J.-H.; Yoo, Y.-S.; Park, J.-W.; Lim, H. C. *Solid State Ionics* **2002**, *149*, 157.
(32) Finnerty, C. M.; Coe, N. J.; Cunningham, R. H.; Ormerod, R. M. *Catal. Today* **1998**, *46*, 137.
(33) Nikolla, E.; Holewinski, A.; Schwank, J.; Linic, S. *J. Am. Chem. Soc.* **2006**, *128*, 11354.
(34) Mi, H.; Xu, Y.; Shi, W.; Yoo, H.; Park, S.; Park, Y.; Oh, S. M. *J. Mater. Chem.* **2011**, *21*, 19302−19309.
(35) Eshkenazi, V.; Peled, E.; Burstein, L.; Golodnitsky, D. *Solid State Ionics* **2004**, *170*, 83−91.